第 44 卷 第 4 期/2024 年 2 月/光学学报 研究论文

光学学报

基于硫铟锌纳米花的被动调Q激光

朱宜璇[1]，仝鲁阳[1]，蔡阳健[1,2]，赵丽娜[1,2**]，郑立仁[1,2*]

[1]山东师范大学物理与电子科学学院，光场调控及应用中心，山东省光学与光子器件技术重点实验室，山东 济南 250358；

[2]华东师范大学与山东师范大学光调控科学与光子集成芯片联合研究中心，上海 200241

摘要 采用溶液法合成了二维硫铟锌纳米花，并测量了其可饱和吸收参数，其中，饱和强度为 675 MW/cm^2，调制深度为 7.8%。通过搭建 1 μm 全固态激光器，获得最大输出功率为 240 mW、最大重复频率为 629.08 kHz、最小脉冲宽度为 388 ns、相应的单脉冲能量为 0.38 μJ、峰值功率为 0.98 W 的脉冲激光。结果表明，由于硫空位的存在，硫铟锌纳米花能够吸收能量低于其带宽的光子，在近红外区域，表现出良好的可饱和吸收特性，且在激光器中，能够获得高重复频率和短脉冲宽度的激光输出。因此，基于硫铟锌纳米材料的可饱和吸收体在调Q脉冲激光器中具有广阔的应用前景。

关键词 非线性光学；脉冲激光；可饱和吸收体；二维材料；硫空位；硫铟锌

中图分类号 TN248.1 **文献标志码** A **DOI**：10.3788/AOS231707

1 引 言

近年来，脉冲激光器在医疗、通信、材料加工等领域有着广泛的应用[1-8]。可饱和吸收体(SA)是触发脉冲操作的关键元件，它可以在超短的时间尺度上通过切换不同的吸收态来产生超快激光[9]。在过去的几年里，各种二维材料(Two-dimensional materials)被应用于超快激光的研究，如石墨烯[10-11]、过渡金属氧化物[12-15]、拓扑绝缘体[16]、黑磷[17-18]和MXenes[19]等。其中过渡金属二硫族化合物(TMDs)是将过渡金属(Mo，W，Ti，Re，Hf)夹在两个硫族(S，Se，Te)平面之间，这种结构具有可靠的光学、机械和电子特性，如今已成为具有较高研究价值的新兴二维材料。因此，TMDs作为可饱和吸收体被广泛应用于脉冲激光器中，如MoS_2[20-24]、ReS_2[25]、WS_2[26]等。然而，TMDs通常具有较高的饱和光强(数十GW/cm^2)[27-28]。最近，三元金属硫化物(TMSs)纳米材料由于具有超宽带非线性光学响应、高载流子迁移率和优异的空气稳定性，成为许多研究人员探索的方向。Bi_2O_2Se是一种二维三元金属硫化物材料，Liu等[29]利用Bi_2O_2Se纳米片作为可饱和吸收体，实现了超短脉冲宽度的高性能锁模激光输出。除Bi_2O_2Se材料外，三元硫化物$ZnIn_2S_4$(ZIS)拥有二维[S-Zn-S-In-S-In-S]层组成的层状结构[30]，具有电子可调谐特性和光学特性[31]。与CdS、Sb_2S_3等传统二元金属硫化物相比，ZIS毒性较小，具有化学稳定性好、制备方法简单、来源丰富等优点[32-33]。在光学性质方面，ZIS具有较高的光吸收系数和较强的光学稳定性[34-37]，现已被广泛应用于光催化领域[38]。此外，由于ZIS中存在丰富的硫空位，其电荷输运特性会发生变化[39]，因此，具有硫空位的层状ZIS可作为高效可饱和吸收体并应用于脉冲激光器中。

本文采用溶液法合成了具有硫空位的ZIS纳米花。利用扫描电镜(SEM)、X射线衍射(XRD)图谱和紫外-可见-近红外光谱(UV-Vis-NIR)分析了ZIS纳米花的形貌、相结构和紫外可见漫反射光谱。利用典型开孔Z扫描技术，研究了ZIS的非线性饱和吸收特性，并搭建激光器验证了ZIS的光学性能和非线性光学响应，最终实现基于ZIS的被动调Q激光输出。

2 ZIS纳米花的制备与表征

ZIS纳米花可以通过溶液法进行制备[38]。首先，将$InCl_3\cdot4H_2O$(0.8 mmol)、$ZnCl_2$(0.8 mmol)、硫代乙酰胺(4.8 mmol)等反应原料溶解于甘油水溶液(54 mL，体积分数为20%)中，经磁力搅拌30 min后，把上述溶液转移到500 mL的圆底烧杯中，并放在80 ℃油浴中进行加热，同时继续磁力搅拌2 h。待原料反应充分后，将烧杯从油浴中取出，静置一段时间。待温度降至室温后，对溶液进行离心，将沉淀物用水和无

收稿日期：2023-10-27；**修回日期**：2023-11-19；**录用日期**：2023-11-27；**网络首发日期**：2023-12-12

基金项目：国家重点研发计划项目(2022YFA1404802，2019YFA0705000)、国家自然科学基金(91950106，12274267，12192254，92250304，11974218)

通信作者：*zlrgym@sdnu.edu.cn；**lnzhao@sdnu.edu.cn

水乙醇洗涤数次，然后放入 60 ℃真空室干燥 18 h，最终得到有缺陷的 ZIS。随后，将 ZIS(4 mg)超声分散到无水乙醇(10 mL)中 1 h，之后将该分散液(200～300 μL)转移到石英衬底上。在室温下待乙醇干燥后，得到 ZIS 可饱和吸收体。

ZIS 纳米花的 SEM 图像如图 1(a)和图 1(b)所示，图 1(a)是在 1 μm 尺度下的照片，图 1(b)是在 200 nm 尺度下的照片。这些纳米花直径为 100～400 nm，由许多大约 10 nm 厚的超薄纳米片组成，超薄纳米片如图 1(b)标注所示，这与之前的文献[35,40]所述一致。图 1(c)为 ZIS 纳米花的 XRD 图谱，通过比对 PDF(Powder diffraction file，PDF# 65-2023)标准卡片，得出图中特征峰与六方结构的 ZIS 的衍射峰相对应[35,38]。ZIS 纳米花的紫外可见漫反射光谱显示其吸收边缘位于 534 nm 处，对应的带隙为 2.32 eV，这与之前的文献[38,41-42]所述一致，如图 1(d)所示。

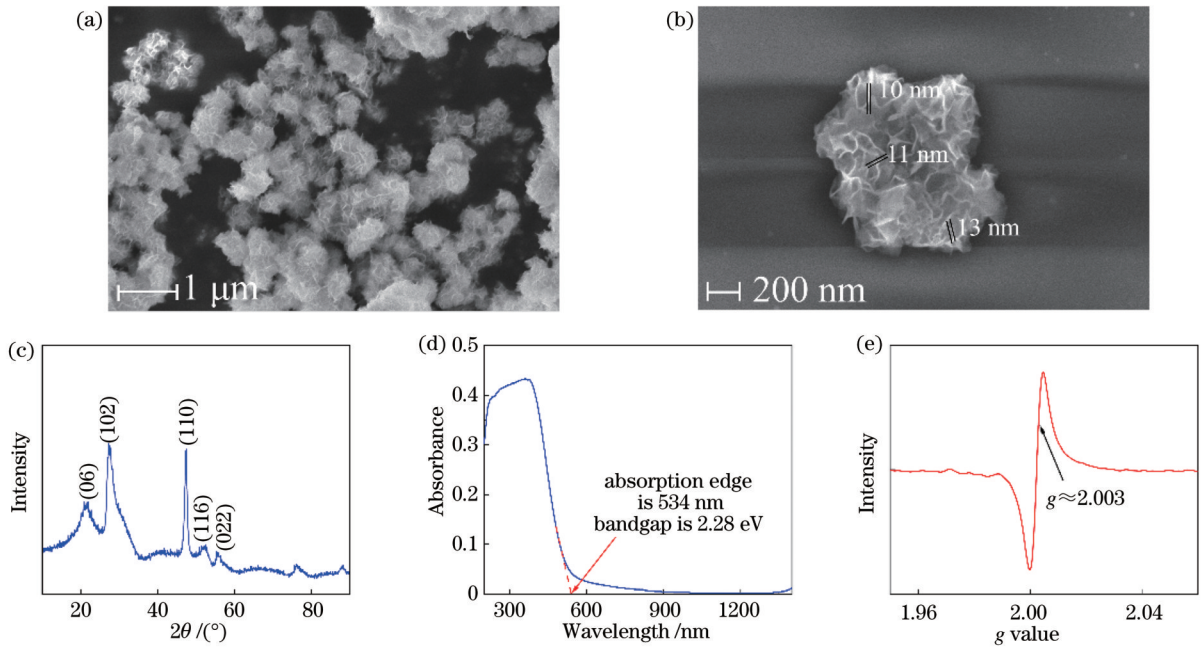

图 1　ZIS 纳米花的特性。(a)在 1 μm 尺度下的 SEM 图像；(b)在 200 nm 尺度下的 SEM 图像；(c)XRD 图谱；(d)吸收谱；(e)EPR 波谱

Fig. 1　Characterization of ZIS nanoflowers. (a) SEM image at 1 μm scale; (b) SEM image at 200 nm scale; (c) XRD spectrum; (d) absorption spectrum; (e) EPR spectroscopy

为了进一步研究 ZIS 纳米花中的硫空位，在液氮(T_0=－183 ℃)真空环境下对 ZIS 进行电子顺磁共振(EPR)波谱测试，结果如图 1(e)所示。当 g=2.003(g 为波谱分裂因子)时，信号强度发生大幅变化，表明在制备的 ZIS 纳米花中存在硫空位[38]。许多关于 ZIS 硫空位的研究发现，硫空位能在其能带中引入中间能级，增强其光吸收能力，并能捕获光生电子，提高光生电荷的输运寿命[30,43]。在其他科研组的研究中，作为可饱和吸收体的少层 MoS_2 显示出可以吸收小于其带隙能量(1.29～1.8 eV)的光(中红外区)，主要原因是存在缺陷，如硫空位[23,44-46]。Wang 等[23]通过理论模拟和实验证实，硫化钼中的硫空位既能保持材料的半导体特性，又能减小材料的带隙宽度，分别在 1.06、1.42、2.10 μm 处实现激光调 Q。在本实验制备 ZIS 的过程中，原料中过量的硫代乙酰胺不仅可以作为硫源，还起到还原剂的作用，使 ZIS 在形成过程中产生硫空位[39,47]。由于 ZIS 具有超薄层状结构，其表面和内部更容易形成硫空位，因此，存在硫空位的 ZIS 可以吸收能量小于其带隙的光子，即波长小于 534 nm 的光子，显示出可饱和吸收特性，在激光器中产生调 Q 激光输出。

3　ZIS 可饱和吸收体的光学性质

为了验证 ZIS 可饱和吸收体的光学性质，首先利用 1064 nm 的皮秒激光器(重复频率为 10 Hz，脉冲宽度为 25 ps)表征 ZIS 的非线性透射率，如图 2 所示。通过逐渐增加入射激光功率，记录相应的透射率与入射

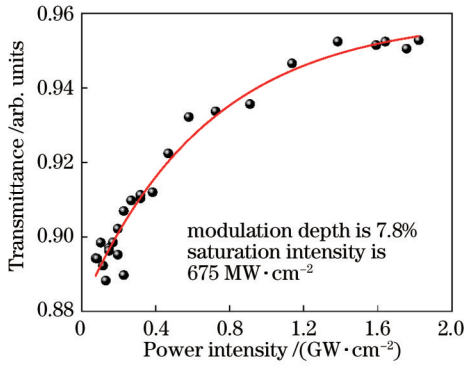

图 2　ZIS 可饱和吸收体的非线性透射率

Fig. 2　Nonlinear transmission of the ZIS saturable absorber

激光强度之间的关系，同时采用可饱和吸收公式拟合了实验数据。

$$T=1-\Delta D\times\exp\left(-I/I_{\mathrm{S}}\right)-\alpha_{\mathrm{ns}},\tag{1}$$

式中：T为透射率；ΔD为调制深度；I和I_{S}分别为入射光强度和饱和光强度；α_{ns}为非饱和损耗。拟合结果表明ZIS可饱和吸收体的饱和强度为675 MW/cm^2，调制深度为7.8%。

其次，验证了ZIS作为可饱和吸收体在脉冲激光器中的调制性能。图3为1 μm脉冲激光实验装置示意图。泵浦光源采用中心波长为808 nm的光纤耦合连续波激光二极管（LD，芯尺寸为200 μm，数值孔径为0.22）。增益介质采用Nd^{3+}掺杂（离子数分数为0.3%）、尺寸为4 mm×4 mm×8 mm的Nd:YVO_4晶体，1∶1光学耦合系统将泵浦光束聚焦到Nd:YVO_4激光晶体中。激光谐振器的腔长为5 cm，由一个平面输入镜（IM）和一个凹面输出耦合器（OC）组成。输入镜上镀有波长为808 nm的增透膜和波长为1.06 μm的高反膜。输出镜的曲率半径R为200 mm，并镀有1.06 μm的部分透射膜，透射率T为5%。通过在激光晶体和OC之间插入ZIS可饱和吸收体来实现脉冲激光输出。

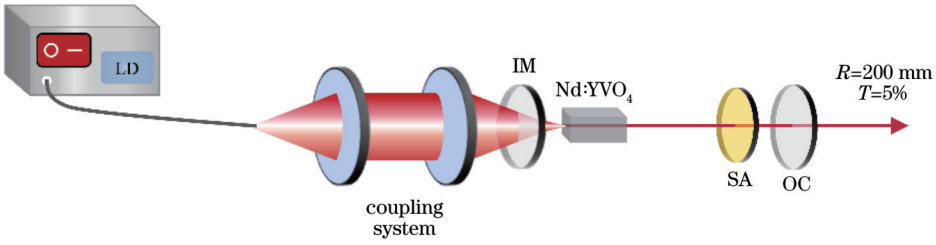

图3　1 μm脉冲激光器的实验装置示意图

Fig. 3　Schematic of the 1 μm pulsed laser experimental setup

首先在泵浦功率为4.10 W时，调节谐振腔使激光的输出功率达到最大，但谐振腔内不放入可饱和吸收体。然后固定谐振腔，研究泵浦功率对输出功率的影响。当泵浦功率为5.31 W时，连续光输出功率达到2.67 W，斜率效率为53.7%，如图4(a)所示。随后通过插入可饱和吸收体并调整其在腔内的位置，使可饱和吸收体处于最佳位置，实现被动调Q激光输出。当泵浦功率为4.10 W时，可获得稳定的调Q脉冲。当泵浦功率增加到5.31 W时，激光器的最大输出功率可达到240 mW。对实验结果进行线性拟合，得到斜率效率为9%，效率较低的主要原因是可饱和吸收体插入谐振腔后造成了损耗。由图4(a)可知，在连续运转状态下，激光最大输出功率可达2.67 W，插入可饱和吸收体后，调Q脉冲激光最大输出功率为240 mW，而可饱和吸收体材料的插入损耗是影响激光斜效率的主要因素。材料制作时的参数会影响损耗，可饱和吸收体材料是在石英衬底上制作完成的，石英衬底的反射损耗、材料的厚度、膜层表面的散射，以及材料吸收层中缺陷和杂质的吸收都会影响可饱和吸收体的光损耗，从而影响腔内的能量，使输出功率变低。

激光器输出的脉冲序列可通过上升时间为150 ps的光电探测器（Thorlabs，DET025AFC，Newton，NJ，USA）和带宽为1 GHz的示波器（LeCroy，HDO4104A，New York，USA）测量得到。脉冲序列很好地反映了脉冲激光的特性。随着泵浦功率的增大，脉冲的重复频率逐渐增大，脉冲宽度逐渐减小。当泵浦源功率从4.10 W增加到5.31 W时，脉冲重复频率从594.6 kHz增大到629.08 kHz，脉冲宽度从560 ns减小到388 ns，如图4(b)所示。由图4(b)可知，本实验所制备的ZIS可饱和吸收体可以实现较高的重

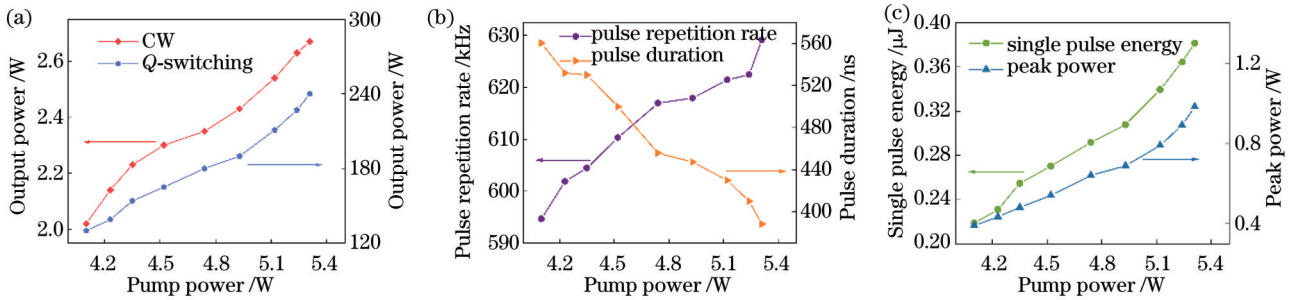

图4　被动调Q激光器的输出参数。(a)连续波（CW）和脉冲激光的输出功率；(b)调Q激光的重复频率和脉冲持续时间；(c)调Q激光的单脉冲能量和峰值功率

Fig. 4　Output performance of the passive Q-switched laser. (a) Output power of continuous wave (CW) and pulsed laser; (b) pulse repetition rate frequency and pulse duration of Q-switched laser; (c) single pulse energy and peak power of Q-switched laser

复频率和较短的脉冲宽度。单脉冲能量和峰值功率可以通过输出功率、脉冲宽度和重复频率计算得到，峰值功率和单脉冲能量随入射泵浦功率的变化关系如图 4(c)所示，可以看出峰值功率和单脉冲能量随泵浦功率的增大而增大。当泵浦功率达到 5.31 W 时，单脉冲能量为 0.38 μJ，对应的峰值功率为 0.98 W。

如图 5 所示，记录了在最大输出功率下脉冲宽度最短的调 Q 激光的脉冲序列。图 5(a)为激光在 20 μs 尺度下的脉冲序列。图 5(b)为脉冲激光在 2 μs 尺度下的脉冲序列，显示出脉冲宽度最短为 388 ns。

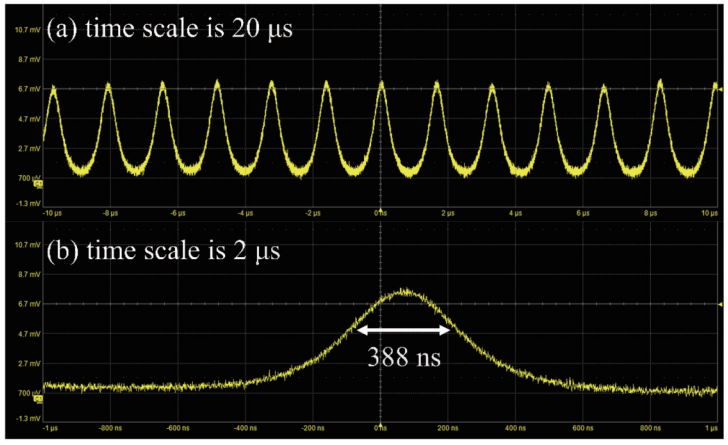

图 5　不同时间尺度下的最短脉冲。(a) 20 μs 时间尺度下的脉冲序列；(b) 2 μs 时间尺度下的脉冲序列

Fig. 5　Shortest pulse at different time scales. (a) Pulse sequence at 20 μs time scale; (b) pulse sequence at 2 μs time scale

脉冲激光的光束质量通过焦距为 150 mm 的聚焦透镜和 CCD(Charge coupled device)相机(Dataray, S-WCD-LCM-C-UV, CA, USA)进行测量。首先测量了谐振腔直接输出的光束情况，光斑能够保持基模高斯分布，激光谐振腔没有输出多模激光。如图 6 中的插图所示，可以看出光斑具有高斯光束轮廓。同时，在聚焦透镜的焦点前后测量了不同位置的光束半径，并拟合出光束质量因子，其中 ω^2 为光束半径的平方，如图 6 所示。通过拟合可以计算出横向光束质量因子(M_x^2)为 1.83，(M_y^2)为 1.65，证明光束在远场(焦点附近)形成的光斑仍保持基模高斯光束分布，也表明脉冲激光具有较高的光束质量。

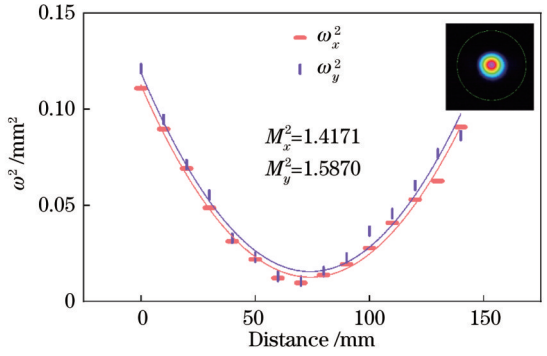

图 6　光束质量因子(插入图为光束轮廓)

Fig. 6　Beam quality factors (insert picture is beam profile)

从图 2 可饱和吸收体的非线性透射率可以看出，硫铟锌纳米花可饱和吸收体的饱和强度为 675 MW/cm^2，调制深度为 7.8%，根据连续锁模条件[48]

$$F_{\mathrm{sat,\,A}}\Delta D<\frac{(PT_{\mathrm{R}})^2\times m\sigma\lambda}{hc\times\pi\omega_{\mathrm{eff,\,L}}^2\times\pi\omega_{\mathrm{eff,\,A}}^2},\tag{2}$$

式中：$F_{\mathrm{sat,\,A}}$ 为饱和光强；P 为激光功率；T_{R} 为光往返一周时间；σ 为激光晶体发射截面；λ 为激光波长；h 为普朗克常量；c 为光速；$\omega_{\mathrm{eff,\,L}}$ 和 $\omega_{\mathrm{eff,\,A}}$ 分别为激光晶体和可饱和吸收体上的有效光斑尺寸；m 为常数项。式(2)左侧为可饱和吸收体参数。制备的可饱和吸收体饱和强度为 675 MW/cm^2，由式(2)可得，若达到连续锁模运转，激光功率要远远高于本实验中的 240 mW，因此，本实验中没有实现锁模。为了达到锁模，需要在实验中优化可饱和吸收体的制备工艺，尽量降低吸收体的饱和光强，或探索饱和强度更低的可饱和吸收体材料，这也是后续要做的工作。

4　结　　论

利用溶液法，合成了二维硫铟锌纳米花，并将其作为可饱和吸收体应用于 Nd:YVO_4 激光器中，实现了调 Q 激光输出，获得了稳定的脉冲序列。在最大泵浦功率为 5.31 W 时，脉冲激光的最大重复频率为 629.08 kHz，脉冲宽度为 388 ns，最大平均输出功率为 240 mW，相应的单脉冲能量为 0.38 μJ，峰值功率为 0.98 W。结果表明，虽然硫铟锌的带隙为 2.32 eV，其吸收边缘位于 534 nm 处，但是在近红外波长区域，由于硫空位的存在，使其能带中引入了中间能级，增强了对近红外波段的光吸收，因此在近红外区域，硫铟锌纳米材料仍然能够表现出良好的可饱和吸收特性，将其应用于激光器中，能够获得高重复频率和短脉冲宽度的激光输出，因此基于硫铟锌纳米材料的可饱和吸收体在调 Q 脉冲激光器中具有广阔的应用前景。

参 考 文 献

[1] Luo Q, Bo F, Kong Y F, et al. Advances in lithium niobate thin-film lasers and amplifiers: a review[J]. Advanced Photonics, 2023, 5(3): 034002.

[2] 雷訇, 刘奇, 王煜, 等. 近衍射极限输出的大芯径尺寸晶体波导被动调Q脉冲激光器[J]. 光学学报, 2021, 41(12): 1214001.
Lei H, Liu Q, Wang Y, et al. Passively Q-switched pulse laser with large core size crystal waveguide near diffraction-limit beam quality output[J]. Acta Optica Sinica, 2021, 41(12): 1214001.

[3] Liu M L, Liu W J, Liu X M, et al. Yttrium oxide as a Q-switcher for the near-infrared erbium-doped fiber laser[J]. Nanophotonics, 2020, 9(9): 2887-2894.

[4] 吴名俊, 谭荣清, 李辉, 等. 高重复频率、窄脉冲声光调Q射频波导CO_2激光器[J]. 中国激光, 2023, 50(22): 2201008.
Wu M J, Tan R Q, Li H, et al. Acousto-optic Q-switched radio frequency waveguide CO_2 laser with high repetition rate and short pulse width[J]. Chinese Journal of Lasers, 2023, 50(22): 2201008.

[5] Li L Q, Kong W J, Chen F. Femtosecond laser-inscribed optical waveguides in dielectric crystals: a concise review and recent advances[J]. Advanced Photonics, 2022, 4(2): 024002.

[6] 夏施君, 许博蕊, 徐鹏飞, 等. 1.3 μm高速直调半导体激光器[J]. 光学学报, 2022, 42(16): 1614001.
Xia S J, Xu B R, Xu P F, et al. 1.3 μm high-speed directly modulated semiconductor laser[J]. Acta Optica Sinica, 2022, 42(16): 1614001.

[7] Cheng Y. First lithium niobate metasurface electro-optic modulator realized[J]. Science China Physics, Mechanics & Astronomy, 2021, 64(4): 240363.

[8] 任俊杰, 贺振兴, 余婷, 等. 2 μm波段纳秒掺铥光纤激光器研究进展[J]. 激光与光电子学进展, 2023, 60(9): 0900003.
Ren J J, He Z X, Yu T, et al. Research progress of 2 μm band nanosecond thulium-doped fiber laser[J]. Laser & Optoelectronics Progress, 2023, 60(9): 0900003.

[9] Keller U. Recent developments in compact ultrafast lasers[J]. Nature, 2003, 424(6950): 831-838.

[10] Soavi G, Wang G, Rostami H, et al. Broadband, electrically tunable third-harmonic generation in graphene[J]. Nature Nanotechnology, 2018, 13(7): 583-588.

[11] Jiang T, Huang D, Cheng J L, et al. Gate-tunable third-order nonlinear optical response of massless Dirac fermions in graphene [J]. Nature Photonics, 2018, 12(7): 430-436.

[12] Guddala S, Kawaguchi Y, Komissarenko F, et al. All-optical nonreciprocity due to valley polarization pumping in transition metal dichalcogenides[J]. Nature Communications, 2021, 12: 3746.

[13] Koo J, Jhon Y I, Park J, et al. Near-infrared saturable absorption of defective bulk-structured WTe_2 for femtosecond laser mode-locking[J]. Advanced Functional Materials, 2016, 26 (41): 7454-7461.

[14] Sun X L, Zhang B T, Li Y L, et al. Tunable ultrafast nonlinear optical properties of graphene/MoS_2 van der Waals heterostructures and their application in solid-state bulk lasers[J]. ACS Nano, 2018, 12(11): 11376-11385.

[15] Jung M, Lee J S, Park J, et al. Mode-locked, 1.94-μm, all-fiberized laser using WS_2-based evanescent field interaction[J]. Optics Express, 2015, 23(15): 19996-20006.

[16] Lee J, Jhon Y I, Lee K, et al. Nonlinear optical properties of arsenic telluride and its use in ultrafast fiber lasers[J]. Scientific Reports, 2020, 10: 15305.

[17] 李黎嘉, 丛春晓. 二维黑磷的光电特性及光电器件研究进展[J]. 发光学报, 2023, 44(6): 995-1005.
Li L J, Cong C X. Optoelectronic properties and photodetection of two-dimensional black phosphorus[J]. Chinese Journal of Luminescence, 2023, 44(6): 995-1005.

[18] 刘邦政, 李双成, 吴政阳, 等. 基于黑磷可饱和吸收体的被动调Q Tm:YAP激光器[J]. 激光与光电子学进展, 2023, 60(1): 0114006.
Liu B Z, Li S C, Wu Z Y, et al. Passively Q-switched operation of Tm:YAP laser with black phosphorus saturable absorber[J]. Laser & Optoelectronics Progress, 2023, 60(1): 0114006.

[19] Jhon Y I, Koo J, Anasori B, et al. Metallic MXene saturable absorber for femtosecond mode-locked lasers[J]. Advanced Materials, 2017, 29(40): 1702496.

[20] Woodward R I, Howe R C T, Hu G, et al. Few-layer MoS_2 saturable absorbers for short-pulse laser technology: current status and future perspectives[J]. Photonics Research, 2015, 3 (2): A30-A42.

[21] Woodward R I, Kelleher E J R, Howe R C T, et al. Tunable Q-switched fiber laser based on saturable edge-state absorption in few-layer molybdenum disulfide (MoS_2) [J]. Optics Express, 2014, 22(25): 31113-31122.

[22] Luo Z Q, Huang Y Z, Zhong M, et al. 1-, 1.5-, and 2-μm fiber lasers Q-switched by a broadband few-layer MoS_2 saturable absorber[J]. Journal of Lightwave Technology, 2014, 32(24): 4679-4686.

[23] Wang S X, Yu H H, Zhang H J, et al. Broadband few-layer MoS_2 saturable absorbers[J]. Advanced Materials, 2014, 26 (21): 3538-3544.

[24] 李平雪, 张光举, 张晗, 等. 反射式二硫化钼可饱和吸收体实现Nd:YVO_4激光器的调Q和调Q锁模输出[J]. 光学学报, 2015, 35(s1): s114003.
Li P X, Zhang G J, Zhang H, et al. Q-switched and Q-switched mode-locking operation from Nd:YVO_4 laser using reflective MoS_2 saturable absorber[J]. Acta Optica Sinica, 2015, 35(s1): s114003.

[25] Lan R J, Liu G H, Zhao B, et al. Pulse energy enhancement in a passively Q-switched Yb:$Lu_{0.74}Y_{0.23}La_{0.01}VO_4$ laser with ReS_2 saturable absorber[J]. Optics Communications, 2022, 504: 127484.

[26] Luan C, Yang K J, Zhao J, et al. WS_2 as a saturable absorber for Q-switched 2 micron lasers[J]. Optics Letters, 2016, 41(16): 3783-3786.

[27] Yu J, Kuang X F, Li J Z, et al. Giant nonlinear optical activity in two-dimensional palladium diselenide[J]. Nature Communications, 2021, 12: 1083.

[28] Huang J W, Dong N N, McEvoy N, et al. Surface-state assisted carrier recombination and optical nonlinearities in bulk to 2D nonlayered PtS[J]. ACS Nano, 2019, 13(11): 13390-13402.

[29] Liu J T, Yang F, Lu J P, et al. High output mode-locked laser empowered by defect regulation in 2D Bi_2O_2Se saturable absorber[J]. Nature Communications, 2022, 13: 3855.

[30] Zheng X L, Song Y M, Liu Y H, et al. $ZnIn_2S_4$-based photocatalysts for photocatalytic hydrogen evolution via water splitting[J]. Coordination Chemistry Reviews, 2023, 475: 214898.

[31] Gou X L, Cheng F Y, Shi Y H, et al. Shape-controlled synthesis of ternary chalcogenide $ZnIn_2S_4$ and $CuIn(S,Se)_2$ nano-/microstructures via facile solution route[J]. Journal of the American Chemical Society, 2006, 128(22): 7222-7229.

[32] Wu Y, Wang H, Tu W G, et al. Petal-like CdS nanostructures coated with exfoliated sulfur-doped carbon nitride via chemically activated chain termination for enhanced visible-light-driven photocatalytic water purification and H_2 generation[J]. Applied Catalysis B: Environmental, 2018, 229: 181-191.

[33] Wang H, Yuan X Z, Wang H, et al. Facile synthesis of Sb_2S_3/ultrathin g-C_3N_4 sheets heterostructures embedded with g-C_3N_4 quantum dots with enhanced NIR-light photocatalytic performance[J]. Applied Catalysis B: Environmental, 2016, 193: 36-46.

[34] Lei Z B, You W S, Liu M Y, et al. Photocatalytic water reduction under visible light on a novel $ZnIn_2S_4$ catalyst

synthesized by hydrothermal method[J]. Chemical Communications, 2003(17): 2142-2143.
[35] Fang F, Chen L, Chen Y B, et al. Synthesis and photocatalysis of $ZnIn_2S_4$ nano/micropeony[J]. The Journal of Physical Chemistry C, 2010, 114(6): 2393-2397.
[36] Ávila-Godoy R, Mora A J, Acosta-Najarro D R, et al. Structure of the quaternary alloy $Zn_{0.6}Mn_{0.4}In_2S_4$ from synchrotron powder diffraction and electron transmission microscopy[J]. Journal of Applied Crystallography, 2006, 39(1): 1-5.
[37] Sriram M A, McMichael P H, Waghray A, et al. Chemical synthesis of the high-pressure cubic-spinel phase of $ZnIn_2S_4$[J]. Journal of Materials Science, 1998, 33(17): 4333-4339.
[38] Si S H, Shou H W, Mao Y Y, et al. Low-coordination single Au atoms on ultrathin $ZnIn_2S_4$ nanosheets for selective photocatalytic CO_2 reduction towards CH_4[J]. Angewandte Chemie (International Ed. in English), 2022, 61(41): e202209446.
[39] Yang R J, Mei L, Fan Y Y, et al. $ZnIn_2S_4$-based photocatalysts for energy and environmental applications[J]. Small Methods, 2021, 5(10): 2100887.
[40] Zhao C X, Zhang Y Z, Jiang H L, et al. Combined effects of octahedron NH_2-UiO-66 and flowerlike $ZnIn_2S_4$ microspheres for photocatalytic dye degradation and hydrogen evolution under visible light[J]. The Journal of Physical Chemistry C, 2019, 123(29): 18037-18049.
[41] Pan Y, Yuan X Z, Jiang L B, et al. Recent advances in synthesis, modification and photocatalytic applications of micro/nano-structured zinc indium sulfide[J]. Chemical Engineering Journal, 2018, 354: 407-431.
[42] Kumar Y, Kumar R, Raizada P, et al. Novel Z-Scheme $ZnIn_2S_4$-based photocatalysts for solar-driven environmental and energy applications: progress and perspectives[J]. Journal of Materials Science & Technology, 2021, 87: 234-257.
[43] Wang J, Sun S J, Zhou R, et al. A review: synthesis, modification and photocatalytic applications of $ZnIn_2S_4$[J]. Journal of Materials Science & Technology, 2021, 78: 1-19.
[44] Zhou K G, Zhao M, Chang M J, et al. Size-dependent nonlinear optical properties of atomically thin transition metal dichalcogenide nanosheets[J]. Small, 2015, 11(6): 694-701.
[45] Zhou W, Zou X L, Najmaei S, et al. Intrinsic structural defects in monolayer molybdenum disulfide[J]. Nano Letters, 2013, 13(6): 2615-2622.
[46] Qiu H, Xu T, Wang Z L, et al. Hopping transport through defect-induced localized states in molybdenum disulphide[J]. Nature Communications, 2013, 4: 2642.
[47] Du C, Zhang Q, Lin Z Y, et al. Half-unit-cell $ZnIn_2S_4$ monolayer with sulfur vacancies for photocatalytic hydrogen evolution[J]. Applied Catalysis B: Environmental, 2019, 248: 193-201.
[48] Zhang Y X, Lu D Z, Yu H H, et al. Low-dimensional saturable absorbers in the visible spectral region[J]. Advanced Optical Materials, 2019, 7(1): 1800886.

Passive *Q*-Switched Laser Based on Zinc Indium Sulfide Nanoflowers

Zhu Yixuan[1], Tong Luyang[1], Cai Yangjian[1,2], Zhao Lina[1,2**], Zheng Liren[1,2*]

[1]*Shandong Provincial Key Laboratory of Optics and Photonic Device, Shandong Provincial Engineering and Technical Center of Light Manipulations, School of Physics and Electronics, Shandong Normal University, Jinan* 250358, *Shandong, China*;

[2]*Joint Research Center of Light Manipulation Science and Photonic Integrated Chip of East China Normal University and Shandong Normal University, Shanghai* 200241, *China*

Abstract

Objective Pulse lasers have a wide range of applications in the medical treatment, communication, material processing, and other fields. Saturable absorber (SA) is a key element in triggering pulse operation, which can switch between different absorption states and produce ultrafast lasers on ultrafast timelines. In the past few years, various two-dimensional materials have been applied to ultrafast laser research, such as graphene, transition metal oxides, topological insulators, black phosphorus, and MXenes. The transition metal dichalcogenides (TMDs) put transition metals (Mo, W, Ti, Re, Hf) sandwiched between two chalcogenides (S, Se, Te) planes. This structure has reliable optical, mechanical, and electronic properties. It has become a new two-dimensional material. As SA, TMDs are widely used in pulse lasers, such as MoS_2, ReS_2, and WS_2. However, TMDs typically have a high saturation light intensity (tens of GW/cm^2). Ternary metal sulfides (TMSs) nanomaterials have been explored by many researchers due to their ultra-wideband nonlinear optical response, high carrier mobility, and excellent air stability. The TMSs $ZnIn_2S_4$ (ZIS) has a layered structure composed of two-dimensional [S-Zn-S-In-S-In-S] layers with tunable electronic and optical properties. Compared with traditional binary metal sulfides such as CdS and Sb_2S_3, ZIS has the advantages of low toxicity, good chemical stability, simple preparation method, and abundant sources. In terms of optical properties, ZIS has a high optical absorption coefficient and strong optical stability. In addition, the charge transport characteristics of ZIS are changed due to the presence of abundant sulfur vacancies. It is necessary to study the layered ZIS with sulfur vacancies as efficient SA.

Methods In this paper, we synthesize ZIS nanoflowers with sulfur vacancies by solution method. The morphology, phase structure, and ultraviolet-visible (UV-Vis) diffuse reflection spectra of ZIS nanoflowers are analyzed by scanning

electron microscopy (SEM), X-ray diffraction (XRD), and ultraviolet-visible-near infrared (UV-Vis-NIR) spectra. The nonlinear SA characteristics of ZIS are studied by the Z-scan method, and the optical performance and nonlinear optical response of ZIS are verified by constructing a pulsed laser experimental setup. Finally, the passive *Q*-switched laser output based on ZIS is realized.

Results and Discussions We represent the characteristics of ZIS nanoflowers and show SEM images of ZIS-SA in Figs. 1(a) and (b), XRD spectrum of ZIS-SA in Fig. 1(c), absorptance of the ZIS-SA in Fig. 1(d), and EPR spectroscopy of the ZIS-SA in Fig. 1(e). As shown in Fig. 2, we verify the optical properties of the SA. The fitting results show that the saturation intensity of the ZIS-SA is 675 MW/cm^2 and the modulation depth is 7.8%. Second, we verify the modulation performance of ZIS as SA in pulsed lasers. Fig. 3 shows the schematic of the 1 μm pulsed laser experimental setup. Fig. 4 shows the output performance of the passive *Q*-switched laser. As shown in Fig. 4(a), when the pump power is 5.31 W, the continuous output power reaches 2.67 W. Passive *Q*-switched laser is achieved by inserting SA and adjusting its position in the cavity so that the SA is in the best position. When the pump power is 4.10 W, a stable *Q*-switched pulse can be obtained. When the pump power is increased to 5.31 W, the maximum output power of the laser is 240 mW. As shown in Fig. 4(b), with an increase in pump power, the pulse repetition rate gradually increases and the pulse width decreases. When the pump power increases from 4.10 W to 5.31 W, and the pulse repetition rate frequency increases from 594.6 kHz to 629.08 kHz, and the pulse width decreases from 560 ns to 388 ns. As shown in Fig. 4(c), single pulse energy and peak power of the *Q*-switched laser. It can be seen that the peak power and single pulse energy increase with the growing pump power. When the pump power is 5.31 W, the single pulse energy is 0.38 μJ, and the corresponding peak power is 0.98 W. As shown in Fig. 5, we record the shortest pulse at different time scales. Fig. 5(a) shows the pulse sequence at a 20 μs time scale, and Fig. 5(b) shows the pulse sequence at a 2 μs time scale. The minimum pulse width is 388 ns. As shown in Fig 6, we measure the beam quality M^2 factors. The transverse beam quality factor (M_x^2) is 1.83 and the longitudinal beam quality factor (M_y^2) is 1.65 which indicate that the *Q*-switched pulse laser has a high beam quality.

Conclusions Two-dimensional zinc sulfide indium nanoflowers are synthesized by solution method. The *Q*-switched Nd∶YVO_4 laser was realized by ZIS as SA. When the maximum pump power is 5.31 W, the maximum pulse repetition rate frequency of the pulsed laser is 629.08 kHz, the pulse width is 388 ns, and the maximum average output power is 240 mW. The corresponding single pulse energy and peak power are 0.38 μJ and 0.98 W. The results show that although the band gap of indium zinc sulfide is 2.32 eV and its absorption edge is located at 534 nm, the presence of sulfur vacancies introduces intermediate energy levels in the near-infrared band and enhances its light absorption. Therefore, the nanomaterials of indium zinc sulfide can still exhibit good saturation absorption characteristics in the near-infrared region. The laser with a high repetition rate and short pulse width can be obtained by ZIS as SA in the laser resonator. Therefore, zinc indium sulfide nanomaterials have a good application prospect in *Q*-switched pulse lasers.

Key words nonlinear optics; pulsed laser; saturable absorber; two-dimensional materials; sulfur vacancy; zinc indium sulfide